Electromagnetically induced absorption in a bichromatic laser field

A. A. Zhukov,[1,2] S. A. Zibrov,[3] G. V. Romanov,[1,3] Y. O. Dudin,[4] V. V. Vassiliev,[3] V. L. Velichansky,[1,3] and V. P. Yakovlev[1]

[1]*Moscow Engineering Physics Institute, Moscow 115409, Russia*
[2]*Institute für Quantenphysik, Universität Ulm, Ulm 89069, Germany*
[3]*P.N. Lebedev Physical Institute of RAS, Moscow 119991, Russia*
[4]*School of Physics, Georgia Institute of Technology, Atlanta, Georgia 30332-0430, USA*

In this paper we describe experimentally and theoretically the increase in the electromagnetically induced absorption (EIA) resonance under the influence of an additional optical field. EIA was observed on the cycling transition of the rubidium D_2 line in the Hanle configuration in the presence of the second-laser field acting on an open transition coupled with a cycling one via a common ground state. We present results obtained for different polarization orientations and propagation directions of the two laser beams. A systematic theoretical analysis based on the optical Bloch equations explains most of the experimental data. A lot of attention is also paid to a qualitative understanding of the EIA—its resonance shape, amplitude, and the response to the additional optical fields.

I. INTRODUCTION

Magneto-optical properties of atomic gases have been studied for many years. Important phenomena such as Hanle effect in the excited and the ground states [1,2] and optical pumping with polarized radiation of resonance lamp [3] have been discovered and efficiently used in metrology of time and frequency [4] and magnetometry [5]. The development of tunable narrow-linewidth lasers gave new experimental possibilities in optical pumping of atoms. An important example is the discovery of coherent population trapping (CPT) made with polychromatic laser radiation [6,7]. The transmission of two optical fields that couple two ground states with a single excited state in a Λ configuration reveals maximum when the frequency difference of the optical fields is equal to the ground state splitting. The effect named electromagnetically induced transparency (EIT) has found many new applications in laser cooling [8], atomic clocks [9], and magnetometers [10]. An unexpected effect was observed when the same technique of probing transmission of resonant gas with bichromatic radiation was used for degenerate ground state levels [11]. While a regular EIT resonance was displayed in the transmission versus frequency difference of the laser fields when the angular momentum of the ground state F_g was greater than or equal to angular momentum of the excited state F_e, it changed the sign for the cycling transition with $F_e = F_g + 1$. It was demonstrated later that this resonance of EIA appeared also for open transitions provided condition $F_e = F_g + 1$ was fulfilled, although the effect was smaller in this case due to hyperfine optical pumping [12]. Meanwhile for a long time there was an alternative and experimentally simpler technique to probe the distribution of populations and coherences in the ground state of atoms. In this technique the two optical fields propagate along magnetic field and have the same frequencies but different orthogonal circular polarizations (Hanle configuration). The transmission of these fields is measured as a function of the magnetic field that varies energy of Zeeman sublevels and violates the CPT condition fulfilled at zero magnetic field.

The experiments carried out in Hanle configuration for Rb and Cs atoms revealed the same signs of resonances: transmission for $F_e \leq F_g$ and absorption for $F_e = F_g + 1$ [13]. A concise review of early works on this subject has been given in [14].

Typically, the contrast of EIA resonance does not exceed 1%. Significant increase in contrast has been found in two works. In one of them [15] a bright narrow resonance of a circularly polarized light was displayed as a function of transverse magnetic field. In the second one, the increase in EIA resonance in Hanle configuration was observed for D_2 line of ^{87}Rb in the standing wave configuration of a single-frequency laser field [16]. The Doppler broadened cycling $(F_g = 2 \rightarrow F_e = 3)$ and open $(F_g = 2 \rightarrow F_e = 2, 1)$ transitions with resonance frequencies $\nu_{2,3}$, $\nu_{2,2}$, and $\nu_{2,1}$, respectively, overlap in the low-frequency hyperfine component of D_2 line of rubidium. The laser frequency was decreased in small steps from the cycling $(\nu_{2,3})$ to the open $(\nu_{2,2})$ transition. For each value of fixed frequency the dependence of absorption on magnetic field was taken. It was natural to expect that the amplitude of EIA resonance should decrease monotonously and change sign with laser frequency approaching the $\nu_{2,2}$ frequency, that is, EIA should turn to EIT. Indeed this was observed in the experiment for all frequencies but a small region in the vicinity of crossover Doppler-free resonance that occurs at $\nu = (\nu_{2,2} + \nu_{2,3})/2$. In this range the amplitude of EIA increased dramatically. Depending on the laser field amplitudes, this increase could reach the value of 25 times.

In the present paper we focus on the study of the increase in EIA observed at cycling transition under influence of additional field acting on coupled open transition. We present experimental results obtained with the use of a second laser tuned to different open transitions of D_1 line for different polarizations of the laser fields and for the cases of copropagating and counterpropagating laser beams and explain these results theoretically. The paper is organized as follows. The experimental part describes interaction of atoms with bichromatic radiation resonant to two adjacent transitions (V configuration). In the first part the bichromatic radiation is pro-
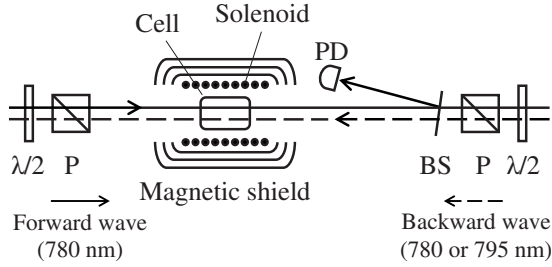
FIG. 1. Experimental setup. P stands for polarizers, BS is a beam splitter (reflects ~8% of incident light), $\lambda/2$ are half wave plates, and PD is a photodetector.

duced for a group of atoms with a specific velocity projection on the laser beams in a standing wave of a single-frequency field tuned to the frequency of the crossover resonance. These atoms see two different resonant frequencies due to the Doppler shifts. The second part describes the experiment carried out by using two independent laser fields which makes the experiment more flexible. The two waves can copropagate or counterpropagate and be tuned to different (D_1 and D_2) lines. Then the theory for the case of the two laser fields tuned in resonance with closed (cycling) and open transitions coupled via common ground state in V configuration is given. It explains variations in the effect for different polarizations and intensities of the laser fields observed in the experiment and predicts its dependence on the involved g factors. The theoretical part also provides detailed physical explanation of both the EIA and the relatively broad structure in its background for the case of a single-laser field. Following [14] we use in explanation a basis in which the quantization axis is parallel to the electric field of laser radiation. Partially these results exactly coincide with those in [14] but we derive them in a simpler way and give more details.

II. EXPERIMENT

The experimental setup is similar for the two parts of the experiment and is shown in Fig. 1. In the first part of the experiment both the forward and the backward waves were formed by one laser working on the D_2 line ($\lambda_{FW} = \lambda_{BW} = 780$ nm) of Rb. In the second part the forward wave was formed by the D_2 laser while the backward wave was formed by an independent D_1 laser ($\lambda_{FW} = 780$ nm, $\lambda_{BW} = 795$ nm). At first we describe results obtained with a single laser.

A. Experiment with a single laser

An extended cavity diode laser [17] was a source of monochromatic (linewidth <1 MHz) and tunable (20 GHz in the vicinity of the D_2 line of Rb) radiation. A part of radiation was split off and directed to the frequency stabilization system (not shown) that utilizes modulation of magnetic field for error signal generation [18].

The energy-level structure of the ^{87}Rb and the involved transitions are shown in Fig. 2. The laser frequency was stabilized to the crossover resonance that occurs via combination of $F_g = 2 \rightarrow F_e = 2$ and $F_g = 2 \rightarrow F_e = 3$ transitions. The ex-
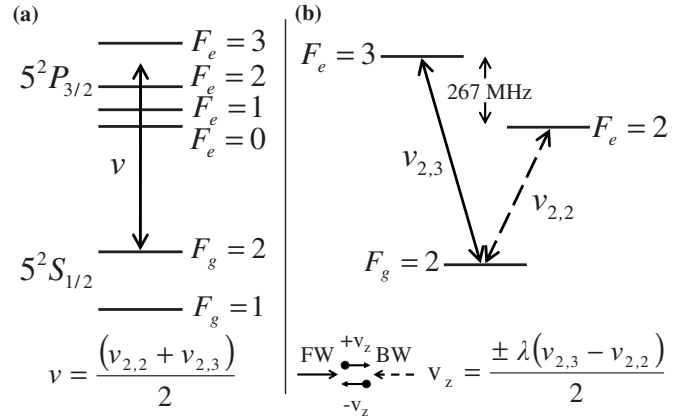
FIG. 2. Energy levels for (a) the D_2 line of ^{87}Rb and (b) the transitions involved in the experiment. FW and BW are forward and backward waves, v is laser frequency, $v_{i,j}$ are the frequencies of the transitions between levels i and j, and v_z is atomic velocity projection on the direction of the light propagation.

periment was carried out with a glass cylindrical cell (60 $\times 55$ mm^2) containing natural mixture of ^{85}Rb (72%) and ^{87}Rb (28%) that was kept at room temperature (23 °C, concentration of $\sim 8.7 \times 10^9$ cm^{-3}). The cell did not contain buffer gases and had no antirelaxation coating of the walls. In order to decrease the laboratory magnetic field and its inhomogeneity a solenoid with the cell inside of it was placed inside a three-layer magnetic shield. The residual magnetic field within the cell dimensions was less than 2 mG. The transmission of the cell was measured for both forward and backward waves as a function of longitudinal magnetic field that was produced by the solenoid. The magnetic field was linearly changed across its zero value.

We studied the influence of the backward wave power on the EIA resonance observed in the forward wave radiation for different polarization orientations of the waves [linear parallel (lin‖lin) and linear orthogonal (lin⊥lin)].

Figure 3 shows the cell transmission of the forward wave tuned to D_2 line for different values of the backward wave power for (a) the lin‖lin and (b) the lin⊥lin cases. The beam diameters were 5 mm, the forward wave power was 1 mW, and the backward wave power was varied from 0 to 1.5 mW. In the following discussion of resonance widths we use both the magnetic field and the frequency scales, which are connected with a coefficient of 0.7 MHz/G (the energy splitting between neighboring Zeeman sublevels of the ground state). The signals presented in Fig. 3 consist of structures of different widths. The wider one stems from the saturation processes and Zeeman splitting and has the width of about the natural width of the excited state. The narrow feature near the zero magnetic field is a level crossing resonance of the ground state (or EIA) and its properties are the main subject of the paper. The displacement of different curves along the ordinate axis is not artificial but corresponds to the actual variation in the baseline. It is clearly seen from Fig. 3(a) that the backward wave increases significantly the amplitude of the EIA resonance in the lin‖lin case. When the polarizations of the waves are linear and orthogonal the influence of the backward wave considerably differs from lin‖lin case: the
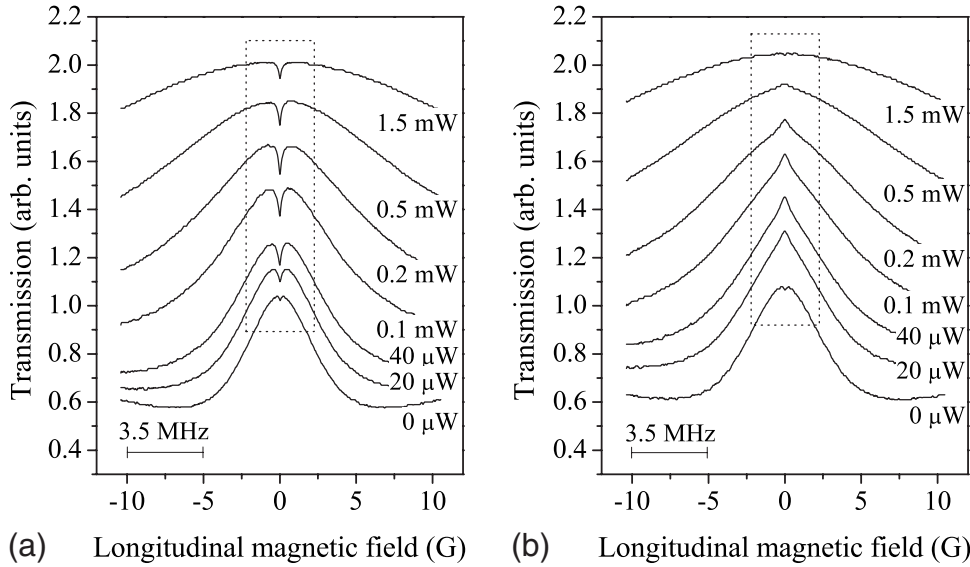
FIG. 3. The cell transmission of the forward wave for different backward wave powers in the case of (a) linear parallel polarizations (lin‖lin) and (b) linear orthogonal polarizations (lin ⊥ lin). The dashed rectangular boxes highlight the EIA resonance.

EIA resonance is smaller and changes its sign two times. In the power range of the backward wave below 40 μW it is a dip in a transmission, then it transforms to a peak, and then again becomes a dip at 1.5 mW of the backward wave laser power [Fig. 3(b)].

Note that for laser frequency tuned to $\nu=(\nu_{2,2}+\nu_{2,3})/2$ both probe and counterpropagating waves interact with two groups of atoms with velocity projections $v_z = \pm \lambda(\nu_{2,3} - \nu_{2,2})/2$. The first group goes in the opposite direction with respect to the probe beam ($v_z < 0$). Here the probe beam is resonant to $F_g=2 \rightarrow F_e=3$ transition, while the counterpropagating wave excites atoms at $F_g=2 \rightarrow F_e=2$ transition. For the second group of atoms moving along the probe beam ($v_z > 0$) interaction is different: the probe beam excites open transition ($F_g=2 \rightarrow F_e=2$) while the backward wave is resonant to the cycling one. In theoretical description we took into account only the first group of atoms. To justify this assumption and to study other geometries and transitions the experiment with two lasers has been carried out.

B. Experiment with two independent lasers

In this part of the experiment we studied the influence of radiation resonant to different open transitions in D_1 line of Rb on the EIA resonance displayed on cycling transition of D_2 line. The experimental setup was essentially the same as in experiment with one laser (Fig. 1) except that the backward wave was formed by the laser tuned to D_1 line (795 nm). The beam diameters were both equal to approximately 5 mm, the forward wave power was 150 μW, and the backward wave power was varied from 0 to 4 mW.

Figure 4 shows the energy levels involved and laser frequencies. Both lasers were tuned to the peaks of the corresponding Doppler broadened lines. In this case only one group of atoms was in resonance with both optical fields ($F_g=2 \rightarrow F_e=3$ transition of the D_2 line and $F_g=2 \rightarrow F_e=2$ or $F_g=2 \rightarrow F_e=1$ transitions of the D_1 line) simultaneously. The transmission spectra of the forward wave for different backward wave powers in the lin‖lin case are shown in Fig. 5. The spectra look practically the same as in the single-laser

experiment [Fig. 3(a)]. For the lin ⊥ lin case transmission spectra also reproduce those depicted in Fig. 3(b). The same results were obtained for copropagating laser beams. A small angle between the beams was introduced in that case in order to separate signal from a probe beam. It was found also that the simultaneous and coordinated off tuning of both laser frequencies from the center of the Doppler line led only to the decrease in the signal without changing its main features. Thus, the results obtained with two lasers confirm that in the case of a single-laser experiment the EIA signal is formed only in one group of atoms in which the forward (probe) and backward waves induce $F_g=2 \rightarrow F_e=3$ and $F_g=2 \rightarrow F_e=2$ transitions, respectively. We note that the influence of the additional field on the EIA signal (displayed in the D_2 line) depends on its polarization and a specific type of the open transition involved. When the second laser is tuned to the $F_g=2 \rightarrow F_e=1$ transition of the D_1 line (instead of the $F_g=2 \rightarrow F_e=2$ transition) the EIA enhancement occurs in the
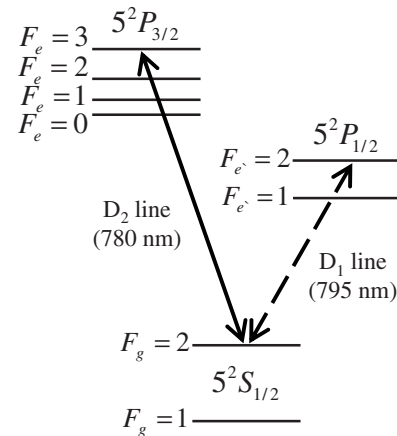
FIG. 4. Level diagram of ^{87}Rb and laser frequencies used in the experiment with two independent laser fields. The forward wave was produced by a laser tuned to the $F_g=2 \rightarrow F_e=3$ transition of the D_2 line, while the backward wave was produced by an independent laser tuned to $F_g=2 \rightarrow F_e=2$ or $F_g=2 \rightarrow F_e=1$ transitions of the D_1 line.
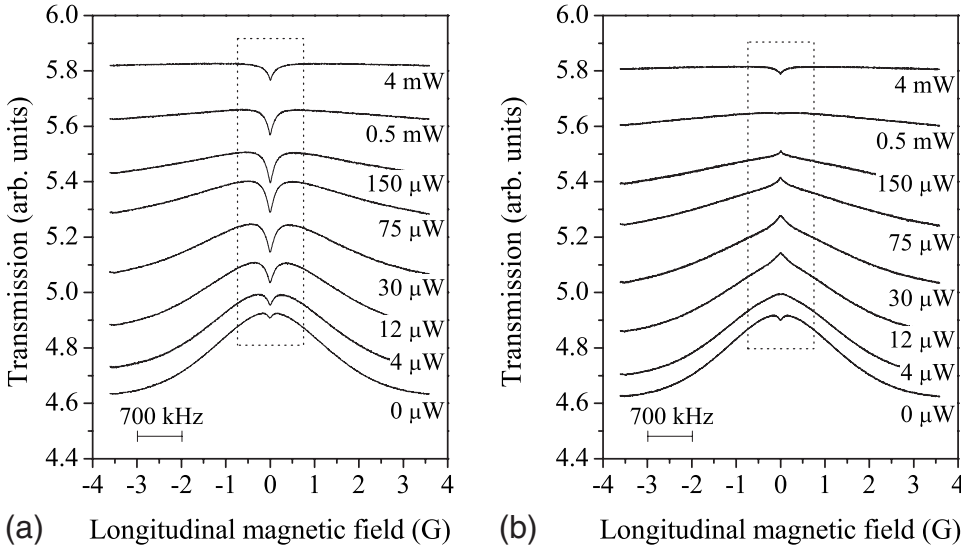
FIG. 5. The transmission of the forward wave for different backward wave powers in the case of (a) linear parallel polarizations (lin∥lin) and (b) linear orthogonal polarizations (lin⊥lin). The dashed rectangular boxes highlight the EIA resonance.

lin⊥lin case while the sign of narrow resonance changes in the lin∥lin case. In other words, changing both the types of the open transition and the polarization of the second field does not vary the dependence of the narrow signal on the second-laser intensity.

It is clear qualitatively that the change in absorption of laser radiation tuned to the cycling transition of D_2 line induced by radiation resonant to D_1 line may occur via changes in coherences and/or in populations of the common ground state sublevels. The σ^+ and σ^- components of polarization in radiation resonant to D_2 line produce Zeeman coherence in the excited state. This coherence is transferred spontaneously to the ground state [19]. The σ^+ and σ^- polarization components of the second-laser field (tuned to D_1 line) also produce the Zeeman coherence in the ground state, which is responsible for the EIT resonance observed for the $F_g = 2 \rightarrow F_e = 2$ transition of the D_1 line. This new coherence can change the transmission of the radiation tuned to D_2 line because both transitions are excited from a common ground state level.

Variations in populations may also contribute to EIA. To see it one has to take into account another ground state sublevel ($F_g = 1$). When the magnetic field is nonzero, D_1 line laser pumps atoms to the $F_g = 1$ state (through the $F_e = 2$ or $F_e = 1$ states) and, consequently, reduces the population of the $F_g = 2$ state. For zero magnetic field a considerable part of atoms is trapped in the dark state (with respect to the D_1 line radiation) and remains in the $F_g = 2$ state. Therefore, the population of the $F_g = 2$ state is greater in the zero magnetic field. The width of this population resonance equals by the order of magnitude to the width of the EIT resonance observed on the D_1 line. This narrow absorption resonance is observed with a D_2 line laser even when it is circularly polarized and does not produce its own coherence. The dependence of amplitude of this resonance on D_1 line laser power is shown in Fig. 6 (circles).

Figure 6 shows that in the case of linearly polarized D_2 line laser radiation the EIA amplitude increases with the D_1 line laser power faster than in the case circularly polarized D_2 line laser light. To describe all these features it is necessary to take into account natural width structures which appear for the linearly polarized radiation and which also

change with increasing in the D_1 line laser power. We give a consistent theoretical analysis of the observed features in the next two parts.

III. THEORY

A. Theory of EIA resonance: Basic equations and the case of a single probe wave

Theoretical description of the effects under consideration is based on a solution of the optical Bloch equations (OBEs) for the density matrix of an atom interacting with two optical waves propagating in opposite directions along a longitudinal magnetic field $\vec{B}$ (Fig. 7). The waves are linearly polarized and the angle between their polarization planes equals α in general case. The forward (probe) and backward (drive) waves are resonant to adjacent atomic transitions having the same $|g, F_g = J-1\rangle$ ground state and different $|e, F_e = J\rangle$ and $|e', F_{e'} = J-1\rangle$ exited states [Fig. 7(a)].

The Rabi frequencies of different induced transitions are given by the products of the values $\Omega = d_a E_a / 2\hbar$, $a = 1, 2$ (where E_a are laser field amplitudes and $d_1 = \langle e, J \| d \| g, J$
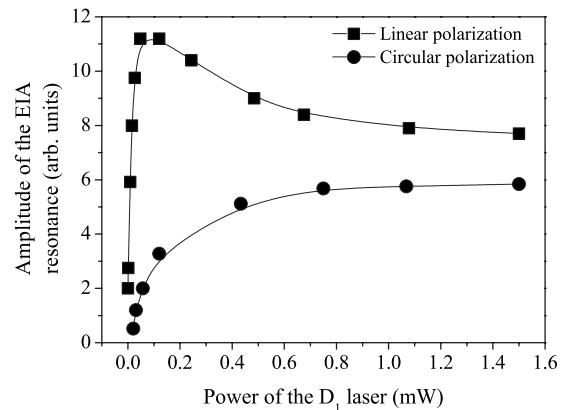
FIG. 6. The amplitude of the EIA resonance vs the laser power tuned to D_1 line ($F_g = 2 \rightarrow F_e = 2$) in the cases of linearly (squares) and circularly (triangles) polarized radiation of laser tuned to the D_2 line ($F_g = 2 \rightarrow F_e = 3$).
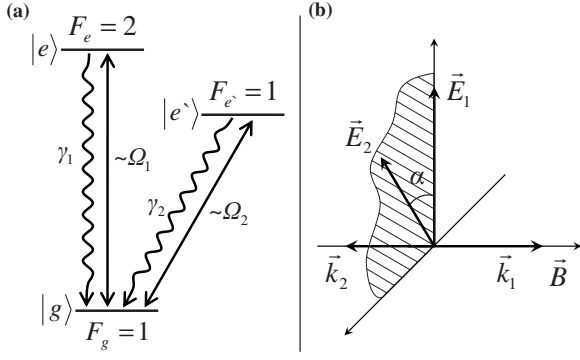
FIG. 7. (a) Three-level scheme of the optical transitions (straight lines) induced by forward ($\sim\Omega_1$) and backward ($\sim\Omega_2$) waves. The wavy lines illustrate the spontaneous emission process. (b) Orientation of the electric field vectors of the two waves relative to the direction of light propagation and the magnetic field vector.

$-1\rangle$ and $d_2 = \langle e', J-1 \| d \| g, J-1 \rangle$ are reduced dipole matrix elements), and the corresponding Clebsh-Gordon coefficients. Both involved transitions, shown in Fig. 7(a), are supposed to be closed, i.e., the exited states $|e\rangle$ and $|e'\rangle$ spontaneously decay only to their common ground state $|g\rangle$ with the rates $\gamma_1 \sim \gamma_2$, respectively. The laser frequencies are tuned to the exact resonance of the corresponding atomic transitions for motionless atoms in zero magnetic field. We recall that $J=3$ in the experiment. However further we mainly focus on the case $J=2$, that is, we take $F_g=1$, $F_e=2$, and $F_{e'}=1$, which provides the simplest model describing the experimental results.

The EIA resonance manifests itself as a narrow peak in the absorption of the probe wave near zero magnetic fields. Amplitude and width of the peak are controlled by the counterpropagating wave. To provide a clear physical interpretation of the resonance it is convenient to use different quantization axes [14]. In the "Hanle basis" with the quantization axis along $\vec{B}$ the magnetic sublevels of the ground and exited states experience Zeeman splitting determined by the values $\hbar\omega_{g,e,e'} = g_{g,e,e'}\mu_B B$, where $g_{g,e,e'}$ denote g factors of the corresponding states and μ_B is Bohr magneton. Optical transitions between these sublevels of the ground and exited states are induced by σ^+ and σ^- polarization components of the respective light fields. When the waves have different linear polarizations the corresponding circular components get a relative phase shift determined by the angle α between polarization planes.

If the axis of quantization is chosen along the electric field of the probe laser wave ("polarization basis") a nonzero magnetic field gives rise to transitions between the substates of the ground state that obey $|\Delta m|=1$ condition, with m being magnetic quantum number. The same happens in each exited state. The transition frequencies are given by $\omega_{g,e,e'}$. We note that in this case the probe wave induces only "vertical" transitions between the states $|g\rangle$ and $|e\rangle$ without change in magnetic quantum numbers. Therefore for the zero magnetic field the two extreme sublevels of the exited state $|e\rangle$ are not involved in the interaction.

Basic equations in the weak saturation regime. Now we consider the weak saturation regime when $\Omega_a \ll \gamma_a$ ($a=1,2$)

for both optical fields and describe the influence of the counterpropagating wave on the narrow structure in the absorption of the probe wave. The EIA resonance occurs in a small vicinity of zero magnetic fields provided Zeeman frequencies obey the conditions

$$\omega_{g,e,e'} \sim \Omega_a^2/\gamma_a \ll \gamma_a. \tag{1}$$

The strong inequalities [Eq. (1)] allow to neglect magnetic field terms in equations for density matrix elements $\rho^{(ee)}$, $\rho^{(ge)}$, $\rho^{(e'e')}$, and $\rho^{(ge')}$ since the equations contain the decay rates γ_1 or γ_2. Moreover, as soon as the time of interaction τ is much greater than $1/\gamma_a$ these elements can be adiabatically eliminated and we arrive at the following set of equations for the ground state density matrix elements $\rho_{mm'}^{(gg)}(m,m'=0,\pm 1) \equiv \rho_{mm'}$ in the Hanle basis:

$$\frac{\partial}{\partial t}\rho_{00} = -\frac{\gamma_1 S_1}{45}[9\rho_{00} - 2(\rho_{11} + \rho_{-1-1} - \rho_{1-1} - \rho_{-11})]$$
$$-\frac{\gamma_2 S_2}{3}\rho_{00}, \tag{2}$$

$$\frac{\partial}{\partial t}\rho_{11} = \frac{\gamma_1 S_1}{90}\left[9\rho_{00} - 5\rho_{11} + \rho_{-1-1} + 2\rho_{1-1} + 2\rho_{-11}\right.$$
$$\left. + \frac{6\Delta_1 i}{\gamma_1}(\rho_{1-1} - \rho_{-11})\right] + \frac{S_2\gamma_2}{6}\left[\rho_{00} - \rho_{11} + \rho_{-1-1}\right.$$
$$\left. + \frac{2\Delta_2 i}{\gamma_2}(e^{-2\alpha i}\rho_{-11} - e^{2\alpha i}\rho_{1-1})\right], \tag{3}$$

$$\frac{\partial}{\partial t}\rho_{-11} = \frac{\partial}{\partial t}\rho_{1-1}^* = \left(2i\omega_g - \frac{\gamma_1 S_1 + \gamma_2 S_2}{3}\right)\rho_{-11}$$
$$-\frac{\gamma_1 S_1}{30}\left(3\rho_{00} + \rho_{-1-1} + \rho_{11} + \frac{2\Delta_1 i}{\gamma_1}(\rho_{11} - \rho_{-1-1})\right)$$
$$-\frac{\gamma_2 S_2}{6}e^{2\alpha i}\left[\rho_{-1-1} + \rho_{11} + \rho_{00} + \frac{2\Delta_2 i}{\gamma_2}(\rho_{-1-1} - \rho_{11})\right]. \tag{4}$$

Here

$$S_a \equiv \frac{|\Omega_a|^2}{\Delta_a^2 + \gamma_a^2/4} \tag{5}$$

denote the two field saturation parameters which depend on the Doppler shifts $\Delta_a = -\vec{k}_a\vec{v} = -k_a v$ due to an atomic velocity v along the laser beams. Since $k_2 \approx -k_1$ the Doppler shifts have opposite signs but practically the same absolute values, i.e., $\Delta_1 \equiv \Delta \approx -\Delta_2$. It is clear that the characteristic values of $|\Delta_a|$ are of the order of γ_a.

Due to the weak saturation regime the interactions with the probe ($\sim S_1$) and driving ($\sim S_2$) fields give additive contributions to Eqs. (2)–(4).

We would like to emphasize that the magnetic field terms ω_g are small according to Eq. (1) and appear only in Eq. (4) for nondiagonal matrix elements. Here they are combined with the parameter $\gamma_1 S_1 + \gamma_2 S_2$. The latter describes the decay rate of the coherence between the ground state sublevels with

$m = \pm 1$. The decay of the coherence is given by the total rate of spontaneous transitions from the states $|e\rangle$ and $|e'\rangle$ to the ground state $|g\rangle$, i.e., by the sum of the excitation probabilities $|\Omega_a|^2/\gamma_a^2$ multiplied by γ_a. In other words, the decay of the coherence induced in the common ground state occurs due to interaction with both optical waves. The values ω_g and $\gamma_1 S_1 + \gamma_2 S_2 \sim |\Omega_a|^2/\gamma_a \ll \gamma_a$ are comparable and their ratio, as we will see below, is responsible for the structure of the EIA resonance. Namely, the width of the central peak is given by the ratio $\omega_g/(\gamma_1 S_1 + \gamma_1 S_2)$ of these parameters. Note that Eqs. (2) and (3) for diagonal matrix elements lead to the conservation law $Sp\rho = W(v)$ for each given atomic velocity described by the distribution function $W(v)$. With the substitution $\rho \to W(v)\rho$, the conservation law for each velocity reads $Sp\rho = 1$.

The angle α between polarization planes results in the relative phase factors $\exp(\pm 2i\alpha)$ that appear in terms describing the influence of the second wave on the nondiagonal density matrix elements in contrast to the terms appearing due to the first field. This result follows immediately from the fact that the polarization planes of the two waves can be obtained from each other via rotation around the axis $\vec{B}$ by an angle of α. Therefore, the corresponding density matrix elements are connected via the unitary operator $\hat{U} = \hat{U}(\alpha, \vec{B})$ generated by this rotation, i.e.,

$$\rho \to \hat{U}\rho\hat{U}^+. \qquad (6)$$

Due to the unitary transformation [Eq. (6)], the nondiagonal matrix elements acquire the phases $\pm 2i\alpha$.

Further simplification is based on the assumption that the interaction time τ is large enough, i.e., $\tau S_a \gamma_a \sim \tau |\Omega_a|^2/\gamma_a \geq 1$, when we can omit the time derivatives and find the stationary solution for Eqs. (2)–(4).

Absorption of the probe field. The absorption coefficient of the probe field is proportional to the population $W_e \equiv \langle Sp\rho^{(ee)}\rangle$ of the exited state $|e\rangle$ integrated with the velocity distribution function $W(v)$. Below we omit, for shortness, the symbol $\langle \cdots \rangle$ of averaging. The population, of course, does not depend on the basis used for calculations, i.e., $W_e \equiv Sp\rho^{(ee)} = Sp\tilde{\rho}^{(ee)}$, where $\tilde{\rho}$ denotes the density matrix in the polarization basis. Now we recall that in this basis the probe wave induces only vertical transitions between the states $|g\rangle$ and $|e\rangle$ without change in magnetic quantum numbers. Provided the conditions given by Eq. (1) are fulfilled the upper state population is determined only by populations $\tilde{\rho}_{mm}^{(gg)}$ of the ground state sublevels. The contributions of the nondiagonal matrix elements $\tilde{\rho}_{mm'}^{(gg)}$ into the upper state population contain an additional small factor ω_g^2 and can be neglected. In such a situation we can easily derive W_e for the transition $F_g = J - 1 \leftrightarrow F_e = J$ with an arbitrary J,

$$W_e = 4S_1 \sum_{m=1-J}^{J-1} \frac{J^2 - m^2}{J(4J^2 - 1)} \tilde{\rho}_{mm}^{(gg)}. \qquad (7)$$

The excitation probability W_e is proportional to the saturation parameter S_1 of the probe field and includes the diagonal matrix elements $\tilde{\rho}_{mm}^{(gg)}$ which depend on ω_g, i.e., on the

magnetic field and on the both saturation parameters S_a. The J-dependant multiples come from the Clebsh-Gordon coefficients.

Equation (7) simplifies when $J = 2$, i.e., $F_g = 1$ and $F_e = 1$. Indeed, by using the symmetry $\tilde{\rho}_{11}^{(gg)} = \tilde{\rho}_{-1-1}^{(gg)}$ and the conservation law, we express the sum in Eq. (7) through the population $\tilde{\rho}_{00}^{(gg)}$ of the single sublevel with the projection $m = 0$ in the polarization basis. Hence in this case we get for W_e,

$$W_e = \frac{2S_1}{5}\left(1 + \frac{1}{3}\tilde{\rho}_{00}^{(gg)}\right). \qquad (8)$$

As we see below the compact expressions [Eqs. (7) and (8)] allow interpreting qualitatively the structure of the EIA resonance in a quite simple way.

Now we remind that the density matrix $\tilde{\rho}$ in the polarization basis is connected with τ in the Hanle basis via unitary operator $\hat{U} = \hat{U}(\pi/2, \vec{E} \times \vec{B})$ generated by the $\pi/2$ rotation around the axis $(\vec{E} \times \vec{B})$, i.e., $\tilde{\rho} = \hat{U}\rho\hat{U}^+$, which gives

$$\tilde{\rho}_{00}^{(gg)} = \frac{1}{2}(\rho_{11}^{(gg)} + \rho_{-1-1}^{(gg)} - \rho_{1-1}^{(gg)} - \rho_{-11}^{(gg)}). \qquad (9)$$

Therefore the absorption coefficient or, strictly speaking, the exited state population [Eq. (8)], being expressed through the density matrix elements $\rho_{mm'}^{(gg)} \equiv \rho_{mm'}$ in the Hanle basis, reads

$$W_e = \frac{2S_1}{5}\left(1 + \frac{\rho_{11} + \rho_{-1-1} - \rho_{1-1} - \rho_{-11}}{6}\right). \qquad (10)$$

In connection with Eq. (10) we would like to make a few remarks: (i) the expression [Eq. (10)] can be derived directly from OBE in the Hanle basis; (ii) due to the weak saturation regime the probability W_e is given by the same combination of the ground state density matrix elements $\rho_{mm'}$ as in the case of a single probe wave described in [14]; and (iii) the formula is rather convenient for concrete calculation of the absorption coefficient because the values $\rho_{mm'}$ are given by the stationary solution for Eqs. (2)–(4) and these equations depend on the magnetic field in a very simple way.

The shape of EIA resonance for a single probe wave. For completeness of the whole picture we briefly recall the known results [14], related to the simplest situation of EIA resonance for a single forward wave. The lowest experimental curves in Figs. 3 and 5 correspond to this case. If the backward wave is switched off, i.e., $S_2 = 0$, the stationary solution for Eqs. (2)–(4) gives

$$\rho_{00} = \frac{2}{9}(\rho_{11} + \rho_{-1-1} - \rho_{1-1} - \rho_{-11}) = \frac{8\omega_g^2 + \frac{4}{5}S_1^2\left(\gamma_1^2 + \frac{4}{5}\Delta_1^2\right)}{44\omega_g^2 + \frac{17}{15}S_1^2\left(\gamma_1^2 + \frac{4}{5}\Delta_1^2\right)}. \qquad (11)$$

Therefore the absorption coefficient [Eq. (10)] finally reads [14]
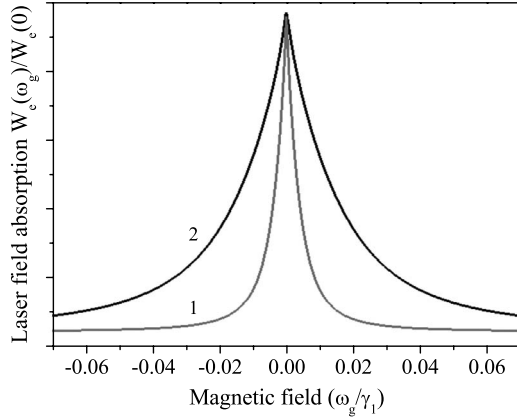
FIG. 8. The shape of the EIA resonance in the case of a single forward wave with Rabi frequency is equal to (1) $|\Omega_1|=0.1\gamma_1$ and (2) $|\Omega_1|=0.2\gamma_1$.

$$W_e = \left\langle \frac{5}{11} S_1 \left(1 + \frac{(1/25)\Gamma^2}{44\omega_g^2 + (17/15)\Gamma^2}\right)\right\rangle, \qquad (12)$$

where $\Gamma^2 = S_1^2(\gamma_1^2 + 4\Delta_1^2/5)$. We also recall that $\langle\cdots\rangle$ denotes the averaging over the velocity distribution $W(v)$. The expression [Eq. (12)] describes the form of the EIA resonance as a function of ω_g in the vicinity of zero magnetic field. Since $|\Delta_1| \sim \gamma_1$, the width $|\omega_g| \sim S_1\gamma_1 \sim |\Omega_1|^2/\gamma_1$ of the narrow structure is proportional to the coherence decay rate. This simple result of the width going down to zero if $|\Omega_1|^2 \to 0$ is true for our model based on a closed atomic transition and a large interaction time τ, i.e., $\tau S_1\gamma_1 \sim \tau|\Omega_1|^2/\gamma_1 \gg 1$. In the case of an open atomic transition the width of a narrow structure is limited by a finite transit time and a decay rate to some nonresonant atomic states.

At zero magnetic field when $\omega_g=0$ the function [Eq. (12)] has the local maximum,

$$W_e(\omega_g = 0) = (8/17)\langle S_1\rangle. \qquad (13)$$

In the field domain $S_1\gamma_1 \ll |\omega_g| \ll \gamma_1$ the function $W_e(\omega_g)$ does not depend on ω_g and reaches its "asymptotic" value,

$$W_e(\infty) = (5/11)\langle S_1\rangle. \qquad (14)$$

To avoid any misunderstandings we note that the asymptotic behavior given by Eq. (14) occurs only in the field domain $S_1\gamma_1 \ll |\omega_g| \ll \gamma_1$ and changes when $|\omega_g| \gtrsim \gamma_1$. The latter domain will be discussed bellow.

As it follows from Eqs. (13) and (14), the contrast of the resonance is about 3%. It does not depend on the field intensity and qualitatively corresponds to experimental data. The ratio $W_e(\omega_g)/W_e(0)$ given by Eqs. (12) and (13) is plotted in Fig. 8 for two values of the Rabi frequency. We see that the

width of the peak increases with Ω_1 while asymptotic values of the ratio $W_e(\omega_g)/W_e(0)$ do not change.

Equation (8) allows explaining the EIA effect, which is why the function W_e has the local maximum at zero magnetic field in a simple way. First of all we note that when $B=0$ the relative probabilities of induced and spontaneous transitions result in the following relation for stationary populations of the ground state sublevels in the polarization basis:

$$\tilde{\rho}_{00}^{(gg)} : \tilde{\rho}_{11}^{(gg)} : \tilde{\rho}_{-1-1}^{(gg)} = 9:4:4. \qquad (15)$$

Hence we have $\tilde{\rho}_{00}^{(gg)}=9/17$ and thus the probability W_e [Eq. (8)] at zero magnetic field $\omega_g=0$ is given by Eq. (13). As it has been mentioned above a weak magnetic field B induces transitions between neighboring sublevels $m=0 \leftrightarrow m=\pm 1$. The transition amplitudes are the same and proportional to a small frequency $\omega_g \sim B$. Since the rate of transitions from a given sublevel is proportional to its population the relation [Eq. (15)] means that the rate of forward transitions $m=0 \leftrightarrow m=\pm 1$ exceeds the rate of backward ones $m=\pm 1 \leftrightarrow m=0$. Therefore the population $\tilde{\rho}_{00}^{(gg)}$ becomes smaller and W_e decreases in the vicinity of $B=0$.

In the case of an arbitrary angular momentum the sum [Eq. (7)] includes $2J-1$ terms. Due to symmetry relations and the conservation law it depends, in fact, on $J-1$ diagonal matrix elements. Nevertheless the above arguments in favor of the local maximum at $B=0$ are still valid.

Now we turn to the asymptotic value given by Eq. (14). This important characteristic parameter of the narrow structure can also be derived in a simple way but in the Hanle basis. Indeed, strong enough magnetic fields satisfying the condition $S_1\gamma \ll |\omega_g| \ll \gamma$ destroy the coherence, i.e., the nondiagonal matrix elements ρ_{-11} and ρ_{1-1} vanish. Therefore, the absorption coefficient [Eq. (10)] depends only on the population ρ_{00}. It can be found from the stationary solution for Eq. (2) in absence of the second wave. By neglecting the nondiagonal matrix elements and using the conservation law we have $\rho_{00}=2/11$ and the probability W_e is given by Eq. (14).

B. Theory: Control of EIA resonance with a counterpropagating wave

Now we turn to our main problem and describe the absorption of a probe wave controlled with the counterpropagating wave acting on the adjacent atomic transition (Fig. 7).

To calculate the absorption coefficient (W_e) [Eq. (10)], we use, as before, the stationary solution for Eqs. (2)–(4). Analytical expression for W_e becomes rather complicated if Doppler shifts are taken into account. Therefore we present here only the result for zero atomic velocity, i.e., $\Delta=0$, when it reads

$$W_e = S_1 \frac{5(1+s)(5+7s)\xi^2 + (3+5s)[8 + s(7 + \cos 2\alpha - \xi \sin 2\alpha)]}{5(1+s)(11+15s)\xi^2 + (3+5s)(17+15s)}. \qquad (16)$$

Here $\xi \equiv 6\omega_g/(\gamma_1 S_1 + \gamma_2 S_2)$ is the dimensionless Zeeman frequency and $s \equiv S_2 \gamma_2/S_1 \gamma_1$ depends on the ratio of field saturation parameters.

The expression for W_e [Eq. (16)] allows us to analyze qualitatively the dependence of the shape of the EIA resonance on the relative intensity of the drive wave for different angles between the polarization planes. The width of the EIA resonance is given by the condition $|\xi| \sim 1$, i.e., $|\omega_g \sim \gamma_1 S_1 + \gamma_2 S_2|$. That is both fields contribute to the width. For an arbitrary angle α the form of the EIA resonance, i.e., the function $W_e(\xi)$, is not symmetric because the nominator has a term linear with respect of ξ. In special cases of parallel ($\alpha=0$) or orthogonal ($\alpha=\pi/2$) polarizations the linear term disappears and $W_e(\xi)$ becomes a symmetric function. The difference between these two situations follows immediately from the structure of Eq. (3). Indeed, if $\alpha=0, \pi/2$ the phase factors $\exp(\pm 2i\alpha) = \pm 1$ are real. Since $\Delta=0$, the two last terms in the right-hand side of Eq. (4) are also real. Therefore, the value of $2 \operatorname{Re} \rho_{-11}$, as well as diagonal matrix elements, which enter the absorption coefficient [Eq. (10)] depends only on ω_g^2. If $\alpha \neq 0, \pi/2$ the phase factors are complex and the function $2 \operatorname{Re} \rho_{-11}$ contains terms with an odd power dependence on $\omega_g \sim B$. These peculiarities are clearly seen when $s \gg 1$ and Eq. (16) simplifies to the form

$$W_e = S_1 \frac{7}{15}\left(1 + \frac{\cos 2\alpha - \xi \sin 2\alpha}{7(\xi^2 + 1)}\right). \quad (17)$$

Following the experiment we now examine in more detail the two special field configurations when the counterpropagating waves have parallel or orthogonal linear polarizations. First of all we note that in these cases the forms of EIA resonance differ dramatically. Indeed, depending on the magnetic field the second term in round brackets in Eq. (17), being positive for $\alpha=0$, becomes negative for $\alpha=\pi/2$. Hence, if the drive wave is strong enough a local maximum at zero magnetic field of $W_e(\xi)$ function for parallel polarizations turns into a local minimum for orthogonal polarizations.

The case of parallel polarizations. Absorption coefficient [Eq. (10)] of the probe wave in the case of parallel polarizations is plotted in Fig. 9 for several intensities of the drive wave. We use the stationary solution for Eqs. (2)–(4) with $\alpha=0$ and Doppler shifts taken into account. The final result for the absorption probability is obtained by averaging over the velocity distribution.

We see that the function $W_e(\omega_g)$ describing the narrow peak in the absorption coefficient increases, as a whole, with intensity of the drive wave. Moreover, the maximum value of the function increases faster than its asymptotic wings and enhances, in that way, the contrast of EIA resonance. Such behavior agrees with experimental results shown in Figs. 3 and 5.

There are simple analytical expressions that describe these two characteristic values of the function $W_e(\omega_g)$ and clearly demonstrate the mentioned properties. So the function has the maximum value

$$W_e(\omega_g = 0) = \left\langle \frac{8}{17} S_1 \left(1 + \frac{2 S_2 \gamma_2}{17 S_1 \gamma_1 + 15 S_2 \gamma_2}\right) \right\rangle \quad (18)$$

at zero magnetic field and reaches the asymptotic value
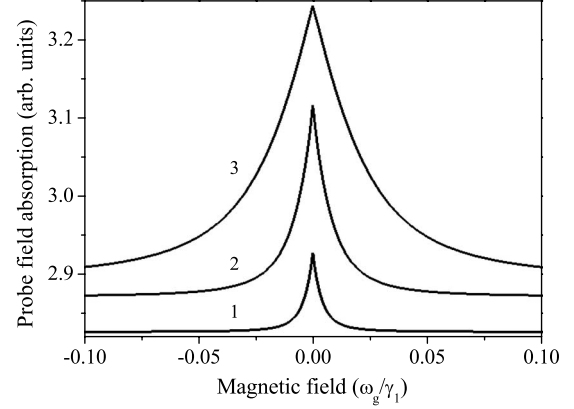
FIG. 9. The shape of the EIA resonance in case of fixed Rabi frequency $|\Omega_1| = 0.1\gamma_1$ of the probe wave and various Rabi frequencies of the backward wave, (1) $|\Omega_2|=0$, (2) $|\Omega_2|=0.1\gamma_1$, and (3) $|\Omega_2|=0.2\gamma_1$, in the case of parallel polarizations ($\alpha=0$) and $\gamma_1=\gamma_2$.

$$W_e = \left\langle \frac{5}{11} S_1 \left(1 + \frac{2}{5} \frac{S_2 \gamma_2}{11 S_1 \gamma_1 + 15 S_2 \gamma_2}\right) \right\rangle \quad (19)$$

in the domain

$$S_{1,2} \gamma_{1,2} \ll |\omega_g| \ll \gamma_{1,2}. \quad (20)$$

If $S_2 \to 0$ Eqs. (18) and (19) coincide with Eqs. (13) and (14) for a single probe wave.

The results given by Eqs. (18) and (19) show, as we already said, that the drive wave increases the absorption of the probe field and enhances the contrast of EIA resonance. The increase saturates when the intensity of the drive field becomes large enough, i.e., $\gamma_1 S_1 \ll \gamma_2 S_2 \ll \gamma$. By using Eqs. (18) and (19) we get then $W_e(\omega_g=0) = (8/15)\langle S_1 \rangle$ and $W_e = (7/15)\langle S_1 \rangle$. Therefore, the maximum contrast is equal to $1/8 \approx 12\%$. This value is about four times larger than that in the case of a single wave.

The role of the drive wave can be easily interpreted in the polarization basis. Since both waves have the same polarization the drive field induces only vertical transitions between sublevels of the ground $|g\rangle$ and exited $|e'\rangle$ states with equal magnetic quantum numbers. If $F_g=F_{e'}=1$ the transition between sublevels with zero projections is forbidden. Therefore the interaction with the drive field leads to increase in $\widetilde{\rho}_{00}^{(gg)}$ due to optical pumping by spontaneous transitions to the sublevel with $m=0$. According to Eq. (8) the absorption of the probe wave depends on the value $\widetilde{\rho}_{00}^{(gg)}$. Hence the increase in the population $\widetilde{\rho}_{00}^{(gg)}$ increases the absorption probability. The less is the magnetic field the more effectively this mechanism works because the field induces an additional mixing of magnetic sublevels.

The case of orthogonal polarizations. Absorption coefficient [Eq. (10)] of the probe wave in the case of orthogonal polarizations is plotted in Fig. 10 for several intensities of the drive wave. The result is based, as before, on the stationary solution for Eqs. (2)–(4), now with $\alpha=\pi/2$, it takes into account Doppler shifts and includes final averaging over atomic velocities.
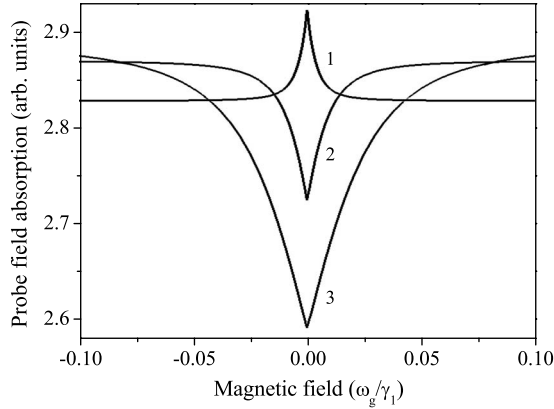
FIG. 10. The shape of the EIA resonance in case of fixed Rabi frequency $|\Omega_1|=0.1\gamma_1$ of the probe wave and various Rabi frequencies of the backward wave, (1) $|\Omega_2|=0$, (2) $|\Omega_2|=0.1\gamma_1$, and (3) $|\Omega_2|=0.2\gamma_1$, in the case of orthogonal polarizations $(\alpha=\pi/2)$ and $\gamma_1=\gamma_2$.

FIG. 11. Dependence of the EIA resonance shape on the angle between polarization planes for fixed Rabi frequencies $|\Omega_{1,2}|=0.1\gamma_1$ of forward and backward waves $(\gamma_1=\gamma_2)$.

We see now that the function $W_e(\omega_g)$ describing the narrow peak in the absorption coefficient exhibits quite different behavior. In particular, the extremum of the function at zero magnetic field reads

$$W_e(\omega_g=0)=\left\langle\frac{8}{17}S_1\left(1-\frac{9}{4}\frac{S_2\gamma_2}{17S_1\gamma_1+15S_2\gamma_2}\right)\right\rangle \quad (21)$$

and coincides, of course, with Eq. (13) if $S_2\rightarrow 0$. In contrast to Eq. (18), the second term in round brackets has the negative sign, and so the extremum of the function decreases when the intensity of the drive wave becomes larger. The asymptotic wings of $W_e(\omega_g)$ in the domain [Eq. (20)] are given by Eq. (19) and increase, as in the case of parallel polarizations, with intensity of the drive wave. Therefore EIA resonance changes its sign for large enough intensities of the drive wave and a dip appears instead of a peak. Such a behavior agrees with experimental results shown in Figs. 3 and 5.

A few lines above we have mentioned that the asymptotic values of $W_e(\omega_g)$ in the domain [Eq. (20)] are described by same Eq. (19) for parallel $(\alpha=0)$ and orthogonal $(\alpha=\pi/2)$ polarizations. This statement is true for any angle between the polarization planes. Indeed, Eqs. (2)–(4) depend on the angle α only via nondiagonal matrix elements that describe the coherence between the ground state sublevels with $m=\pm 1$. In the domain given by Eq. (20) the magnetic field is strong enough and destroys the coherence. Therefore nondiagonal matrix elements tend to zero and the dependence on the angle α disappears.

When the intensity of the drive field becomes large enough, i.e., $\gamma_1S_1\ll\gamma_2S_2\ll\gamma_{1,2}$, the two characteristic values of the function $W_e(\omega_g)$ given by Eqs. (21) and (19) saturate. The minimum value at zero magnetic field is equal to $W_e(\omega_g=0)=(2/5)\langle S_1\rangle$. Since the asymptotic values do not change in comparison to the case $\alpha=0$, i.e., $W_e=(7/15)\langle S_1\rangle$, the contrast is $1/6\approx 17\%$.

To describe qualitatively the influence of the drive wave on the absorption coefficient we return to the polarization basis. Linear polarization of the wave acting on the transition $F_g=1\leftrightarrow F_{e'}=1$ is orthogonal to the quantization axis. In this case the σ^+ and σ^- fields induce optical transitions leading to decreasing the population $\tilde{\rho}_{00}^{(gg)}$ of the sublevel with $m=0$ due to the pumping of extreme sublevels with $m=\pm 1$. In particular, in absence of the probe wave and magnetic field the interaction would result in the well known effect of EIT when the sublevel $m=0$ is empty and we meet a pure Λ scheme with a "dark state." Therefore, according to Eq. (8), in presence of the orthogonally polarized drive wave the absorption of the probe wave decreases. The EIA resonance for the forward wave is controlled by the effect of EIT for the backward wave whose influence increases with intensities. It is necessary to emphasize that such a simple interpretation is true in the domain of zero or very small magnetic fields. Nonzero magnetic fields, as well as the probe wave itself, destroy the dark state and cause the increasing of absorption. That is why for large enough drive fields the structure of EIA resonance looks like a dip with the minimum value at zero magnetic field.
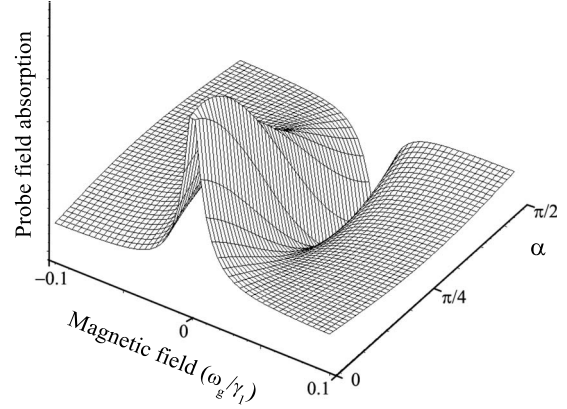
The case of arbitrary angles. As we have already seen from Eqs. (16) and (17), written for zero atomic velocities along laser beams, the shape of EIA resonance becomes more complicated if $\alpha\neq 0,\pi/2$. Thus, there appear contributions having the dispersion form due to the terms with an odd power dependence on the magnetic field. The dependence of the shape of EIA resonance on the parameters of the drive wave, that is, the functions $W_e(\omega_g,\alpha)$ for the fixed intensity of the second wave and $W_e(\omega_g,|\Omega|^2)$ for the fixed angle α, is shown in Figs. 11 and 12.

These results demonstrate that an angle between polarization planes together with an intensity of the drive wave provide us with an effective tool to control the shape of EIA resonance.

The case of $F_g=1\leftrightarrow F_{e'}=0$ transition. In the experiment with the backward light wave acting on the atomic transition $F_g\leftrightarrow F_{e'}=F_g-1$ it was found that parallel and orthogonal polarizations switched the roles in comparison with the above situation. Namely, the absorption coefficient at the center increases for orthogonal polarizations and exhibits the sign change in the case of parallel polarizations.
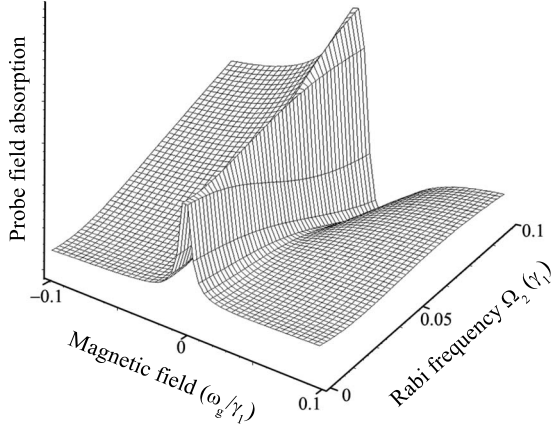
FIG. 12. Dependence of the EIA resonance shape on the Rabi frequency $|\Omega_2|/\gamma_1$ of the backward wave for the fixed angle $\alpha = \pi/2$ between polarization planes. Rabi frequency of the probe wave is equal to $|\Omega_1| = 0.1\gamma_1$ and $\gamma_1 = \gamma_2$.

We discuss qualitatively the simplest case when the drive wave acts on the transition $F_g = 1 \leftrightarrow F_{e'} = 0$. We remind that in the polarization basis the absorption coefficient [Eq. (8)] depends only on the population $\widetilde{\rho}_{00}^{(gg)}$ of the ground state sublevel with $m = 0$. In the case of parallel polarizations the single vertical transition induced by the drive wave results in optical pumping of extreme ground state sublevels with $m = \pm 1$ and decreasing the population $\widetilde{\rho}_{00}^{(gg)}$. Hence, the absorption coefficient decreases and the resonance can change its sign. In the case of orthogonal polarizations transition induced by the $\sigma^+ - \sigma^-$ configuration of the drive wave leads to optical pumping of the sublevel with $m = 0$ and the absorption coefficient increases.

Broad structure of the absorption coefficient. Magnetic field dependence of absorption exhibits not only a narrow peak in the vicinity of $B = 0$ but also a broad structure corresponding to Zeeman shifts $\mu_B B/\hbar$ of the order of optical resonance width γ. Experimental curves in Figs. 2 and 4 clearly show the broad structure in the domain $\mu_B B/(\hbar\gamma) \geq 1$. In most of the published papers theory of this structure is omitted since its full analytical description for two counterpropagating waves gives rather cumbersome expressions even for $F_g = 1 \leftrightarrow F_e = 2, F_{e'} = 1$ transitions. Therefore, for qualitative understanding of this structure we consider the asymptotic behavior of the absorption coefficient for large magnetic fields in the case of a single probe wave,

$$\gamma \ll \omega_{g,e} \ll kv_T, \tag{22}$$

where kv_T is the Doppler width. Here and below we omit the index 1 related to the probe wave.

In this case Zeeman shifts of magnetic sublevels exceed the optical resonance width. Hence, in the weak saturation regime, $\Omega \ll \gamma$, every induced transition between corresponding sublevels of the ground and exited states ($m \leftrightarrow m \pm 1$) occurs mainly in atoms having the resonant velocities $\Delta \approx m(\omega_e - \omega_g) \pm \omega_e$. Here a manifold of induced transitions is decomposed to a set of independent two-level atomic systems with different resonant velocities. Generally speaking these two-level systems are not closed with respect to spon-

taneous transitions. Any spontaneous transition from the upper state of a given two-level system, i.e., of an atom with a given resonant velocity, to the ground state of another two-level system removes the atom from the resonance. The two exceptions are connected with the atomic transition $|1,1\rangle_g \leftrightarrow |2,2\rangle_e$ having the resonant velocity ($\Delta = 2\omega_e - \omega_g$) and the transition $|1,-1\rangle_g \leftrightarrow |2,-2\rangle_e$ corresponding to the opposite velocity. It is clear that these two-level systems are closed with respect to spontaneous transitions. Therefore the main contributions to W_e come from populations $\rho_{22}^{(ee)}(\Delta)$ and $\rho_{-2-2}^{(ee)}(\Delta) = \rho_{22}^{(ee)}(-\Delta)$ of the two marginal sublevels, while the other diagonal elements are negligibly small. In its turn the matrix element $\rho_{22}^{(ee)}$ is determined only by the ground state population $\rho_{11}^{(gg)} \equiv \rho_{11}$ and reads

$$\rho_{22}^{(ee)} = \tfrac{2}{5}S(B)\rho_{11}, \tag{23}$$

where the saturation parameter

$$S(B) = \frac{|\Omega|^2}{(2\omega_e - \omega_g - \Delta)^2 + \gamma^2/4} \tag{24}$$

depends now, in contrast to Eq. (5), on Zeeman shifts ω_e and ω_g for excited and ground states.

The population ρ_{11} can be found from the stationary solution for the ground state OBEs. Since nondiagonal matrix elements contain nonresonant denominators they are small in the parameter $|\Omega|^2/\omega_{g,e}^2 \ll 1$ and can be neglected. Therefore, we deal with simple balance equations. The solution $\rho_{11}(\Delta)$ of these equations smoothly changes in the wide enough range $|\Delta| \sim \omega_{g,e} \gg \gamma$ of velocities. However we see from Eqs. (23) and (24) that only the resonant velocities $\delta = |2\omega_e - \omega_g - \Delta| \sim \gamma \ll \omega_{g,e}$ contribute to the absorption probability W_e. After averaging over the velocity distribution we arrive at

$$W_e = \tfrac{4}{5}\langle S(B)\rho_{11}\rangle \approx \tfrac{4}{5}\rho_{11}(\delta = 0)\langle S\rangle. \tag{25}$$

Hence, in the asymptotic domain of magnetic fields [Eq. (22)], the absorption coefficient reaches a constant value given by Eq. (25).

The value $\rho_{11}(\delta = 0)$ reads

$$\rho_{11}(\zeta) = \left(1 + \frac{5(\zeta-1)^2}{3}\frac{3(\zeta-1)^2 + (\zeta-3)^2}{(\zeta-1)^2 + 5(\zeta-3)^2}\right)^{-1}, \tag{26}$$

where $\zeta = g_g/g_e$. This result means that the absorption probability W_e depends only on the ratio of g factors of the ground and exited states. In particular, for equal g factors, i.e., $\zeta = 1$, we get $\rho_{11} = 1$ and $W_e = (4/5)\langle S\rangle$. The latter exceeds the local maximum of the central peak given by Eq. (13), i.e., the value $W_e(B = 0) = (8/17)\langle S\rangle$.

It is interesting to note that the value of ρ_{11} [Eq. (26)] strongly depends on the sign of ζ, i.e., on the relative positions of Zeeman shifts for the ground and exited states. For instance, if $\zeta = -1$ we have $\rho_{11} = 9/29$ and $W_e \approx (1/4)\langle S\rangle$ which is smaller than $W_e(B = 0)$. It means that in this case the broad structure changes its "sign" (Fig. 12).

The results of numerical calculations of the absorption coefficient in the weak saturation regime are shown in Fig. 13. Shape of the curves exhibits both the narrow structure of the EIA resonance in the vicinity of $B = 0$ (it is shown also in the inset) and a broad structure in a wide domain of magnetic
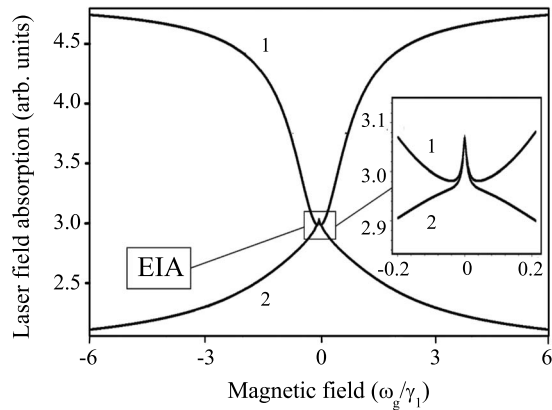
FIG. 13. Dependence of the absorption coefficient on the magnetic field for two sets of g factors: (1) $g_g=1/2, g_e=2/3$ and (2) $g_g=-1/2, g_e=2/3$. The Rabi frequency is equal to $|\Omega_1|=0.1\gamma_1$. The inset shows the narrow structure of EIA resonance at a larger scale.

fields. We see that the two curves calculated for an opposite sign of the ratio g_g/g_e differ dramatically. Note that g factors $(g_g=1/2, g_e=2/3)$ used for the curve 1 correspond, in fact, to the transition $F_g=2 \leftrightarrow F_e=3$ in ^{87}Rb and have been chosen just for convenience.

As it is known there is another contribution to the broad (natural) structure of the signal in Hanle configuration, which stems from stimulated Hanle effect [20] whose origin is similar to that of Lamb dip. It appears since saturation in a single group of atoms in a running linearly polarized wave at zero magnetic field is greater than the saturation in two groups of atoms interacting with two circularly polarized waves when splitting in magnetic field exceeds natural width. We have considered in theory low intensities of laser

fields and have neglected the saturation due to atoms pumped to the excited state. However, in real atom there is stronger saturation mechanism connected to the optical pumping of atoms into another hyperfine sublevel of the ground state. We have not considered this known contribution to broad structure since our "model atom" does not have another hyperfine sublevel of the ground state (a closed system approach).

IV. CONCLUSION

The dependence of EIA signal observed at cycling transition of ^{87}Rb D$_2$ line in Hanle configuration on parameters of additional field applied to an adjacent open transition in V scheme has been studied in detail experimentally. We have found that subnatural and natural structures (in terms of the width of the excited P state) are very sensitive to intensity and polarization of additional field and specific type of the open transition involved, that is, whether it is $F_g=2 \rightarrow F_e=2$ or $F_g=2 \rightarrow F_e=1$. On the contrary, it is not sensitive to geometry (copropagating or counterpropagating beams) and to the wavelength of transition resonant to the second field (780 or 794 nm). Most of the experimentally observed results are in good agreement with theory based on OBEs in spite of the fact that theory has been developed for a system with reduced F numbers. We have analyzed behavior of both subnatural and natural structures in signal and have given physical explanation for most features of the observed effects. Some new properties such as dependence on g factors and dispersionlike signals for arbitrary angle between linear polarizations of two laser fields have been predicted by theory. Preliminary experiments confirmed the first prediction. To check the dependence on g factors we need experiments with other atoms.

[1] W. Hanle, Z. Phys. **35**, 346 (1926).

[2] C. Cohen-Tannoudji, J. Dupont-Roc, S. Haroche, and F. Laloë, Phys. Rev. Lett. **22**, 758 (1969).

[3] A. Kastler, J. Phys. Radium **11**, 255 (1950); J. Brossel and F. BitterPhys. Rev. **86**, 308 (1952); W. Happer, Rev. Mod. Phys. **44**, 169 (1972).

[4] J. Vanier and C. Audoin, *The Quantum Physics of Atomic Frequency Standards* (Adam Hilger, New York, 1989).

[5] E. B. Alexandrov and V. A. Bonch-Bruevich, Opt. Eng. **31**, 711 (1992).

[6] G. Alzetta, A. Gozzini, L. Moi, and G. Orriolis, Nuovo Cimento Soc. Ital. Fis., B **36**, 5 (1976).

[7] E. Arimondo, Prog. Opt. **35**, 257 (1996).

[8] Harold J. Metcalf and Peter van der Straten, *Laser Cooling and Trapping* (Springer-Verlag, New York, 1999).

[9] S. Knappe, P. D. D. Schwindt, V. Shah, L. Hollberg, J. Kitching, L. Liew, and J. Moreland, Opt. Express **13**, 1249 (2005).

[10] P. D. D. Schwindt, S. Knappe, V. Shah, L. Hollberg, J. Kitching, L. Liew, and J. Moreland, Appl. Phys. Lett. **85**, 6409 (2004).

[11] A. M. Akulshin, S. Barreiro, and A. Lezamo, Phys. Rev. A **57**, 2996 (1998).

[12] A. S. Zibrov and A. Matsko, JETP Lett. **82**, 472 (2005).

[13] Y. Dancheva, G. Alzetta, S. Cartaleva, M. Taslakov, and Ch. Andreeva, Opt. Commun. **178**, 103 (2000).

[14] F. Renzoni, C. Zimmermann, P. Verkerk, and E. Arimondo, J. Opt. B: Quantum Semiclassical Opt. **3**, S7 (2001).

[15] F. Renzoni, S. Cartaleva, G. Alzetta, and E. Arimondo, Phys. Rev. A **63**, 065401 (2001).

[16] S. A. Zibrov, Ya. O. Dudin, A. G. Radnaev, V. V. Vassiliev, V. L. Velichansky, D. V. Brazhnikov, A. V. Taichenachev, and V. I. Yudin, JETP Lett. **85**, 417 (2007).

[17] V. V. Vassiliev, S. A. Zibrov, and V. L. Velichansky, Rev. Sci. Instrum. **77**, 013102 (2006).

[18] A. V. Yarovitsky *et al.*, Quantum Electron. **34**, 341 (2004).

[19] A. V. Taichenachev, A. M. Tumaikin, and V. I. Yudin, Phys. Rev. A **61**, 011802(R) (1999).

[20] W. Demtröder, *Laser Spectroscopy*, 3rd ed. (Springer-Verlag, Berlin, 2003), Chap. 12.